BJRS

BRAZILIAN JOURNAL
OF
RADIATION SCIENCES
07-02A (2019) 01-19

SBPR
Sociedade Brasileira de Proteção Radiológica

Microbeam X-ray fluorescence mapping of Cu and Fe in human prostatic carcinoma cell lines using synchrotron radiation

K. M. J. Rocha[a]., R. G. Leitão[b]., E. G. Oliveira-Barros[c]., M. A. Oliveira[c]., C. G. L. Canellas[b]., M. J. Anjos[b]., L. E. Nasciutti[c]., R. T. Lopes[a].

[a] *Nuclear Instrumentation Laboratory/Federal University of Rio de Janeiro/21941-450, Rio de Janeiro, Rio de Janeiro, Brazil*

[b] *Physics Institute/Stated University of Rio de Janeiro/20550-900, Rio de Janeiro, Rio de Janeiro, Brazil*

[c] *Institute of Biomedical Sciences/Federal University of Rio de Janeiro/21044-020, Rio de Janeiro, Rio de Janeiro, Brazil*

e-mail_kjose@nuclear.ufrj.br

ABSTRACT

Cancer is a worldwide public health problem and prostate cancer continues to be one of the most common fatal cancers in men. Copper plays an important role in the aetiology and growth of tumours however, whether intra-tumoral copper is actually elevated in prostate cancer patients has not been established. Iron, an important trace element, plays a vital function in oxygen metabolism, oxygen uptake, and electron transport in mitochondria, energy metabolism, muscle function, and hematopoiesis. The X-ray microfluorescence technique (µXRF) is a rapid and non-destructive method of elemental analysis that provides useful elemental information about samples without causing damage or requiring extra sample preparations. This study investigated the behavior of cells in spheroids of human prostate cells, tumour cell line (DU145) and normal cell line (RWPE-1), after supplementation with zinc chloride by 24 hours using synchrotron X-ray microfluorescence (µSRXRF). The measurements were performed with a standard geometry of 45º of incidence, excited by a white beam using a pixel of 25 µm and a time of 300 ms/pixel at the XRF beamline at the Synchrotron Light National Laboratory (Campinas, Brazil). The results by SRµXRF showed non-uniform Cu and Fe distributions in all the spheroids analyzed.

ISSN: 2319-0612
Accept Submission: 2018-12-12

Keywords: X-Ray, microfluorescence, cancer.

1. INTRODUCTION

Prostate cancer is considered the second most common in the male population worldwide and ranks 15th in cancer deaths in men, accounting for about 6% of the world's total cancer deaths [1]. Copper levels are increased in the tumour tissue of patients affected by prostate cancer (PCa). The molecular mechanisms in which tumor cells proliferate in the presence of elevated levels of copper are therefore of paramount importance for understanding the progression of tumor growth [2]. Copper is a potent prooxidant and excess causes the generation of cytotoxic reactive oxygen species (ROS) in cells. The differential response between normal and cancerous cells to elevated intracellular copper is the premise for the development of copper-ionophores endowed with anticancer properties [3,4]. It is not established, however, to what extent copper is needed for prostate cancer cells, Duke University initiated in 2017 a phase 1 clinical trial based on the propensity of prostate cancer cells for copper [5].

Iron deficiency and iron deficiency-associated anemia are common complications in cancer patients. Most iron deficient cancer patients present with functional iron deficiency (FID), a status with adequate storage iron, but insufficient iron supply for erythroblasts and other iron dependent tissues [6].

Zinc is the second most common trace metal in the human body and is required for the normal growth, proliferation, metabolism, and functions of all cells. All cells maintain the cellular concentration of zinc and its intracellular distribution that is optimal for their normal activities. This is achieved by cellular homeostatic processes that maintain their required zinc status; and deviations from the normal zinc range will result in dysfunctional and cytotoxic effects. The human prostate gland contains extremely high levels of zinc, which is due to the specialized zinc accumulating acinar epithelial cells of the peripheral zone. These cells evolve in their unique capability to produce and secrete extremely high levels of citrate, which is achieved by the high-cellular zinc level effects

on the cell metabolism [7,8]. The loss of Zn accumulation is the most consistent and persistent characteristic of prostate malignancy [9].

X-ray microfluorescence (μXRF) technique is a modern tool for examining elemental composition of various types of samples. An important advantage of the μXRF technique is that the primary beam can be focused down to a very small size, allowing small structural features to be analyzed. This technique allows subcellular resolution of multiple elements, provides semiquantitative results down to a few parts per million, and has been applied to numerous organic and inorganic samples [10,11].

The objectives of this study were to analyze Cu and Fe and distributions in spheroids of human prostate cells, tumour cell line (DU145) and normal cell line (RWPE-1), after supplementation with zinc chloride in the following concentrations 0, 50, 100 and 150 μM by 24 hours using synchrotron X-ray microfluorescence (μSRXRF).

2. MATERIALS AND METHODS

2.1. Cell culture and spheroids

Cell spheroids, self-organizing spherical aggregates of cell colonies, were established from a human prostate tumor cell line, DU145, an independent androgen cell line with low metastatic potential, as well as from a normal human prostate epithelial immortalized cell line, RWPE-1. Solid tumors grow in a three-dimensional spatial matrix and their cells are exposed to nonuniform distributions of oxygen and nutrients. To design more adequate in vitro systems that take into account the three-dimensional arrangement of these tumors, cellular spheroids were developed. In fact, spheroids represent very realistically the three-dimensional growth and cell organization of tumors and much more accurately simulate cell-cell interactions and the microenvironmental conditions found in these tumors than cells grown in monolayer [12].

The cell lines were routinely maintained in appropriate culture medium (mixture of salts enriched with amino acids, vitamins, and other essential components for cell growth), RPMI (Roswell Park Memorial Institute) with 10% fetal bovine serum (Gibco) for tumorigenic cell line, and

keratinocyte-SFM (KSF9; Gibco) for normal cell line. The culture was routinely maintained at 37 °C in a 5% CO2 humidified environment. The cell spheroids were established from the cultivation of 2 × 104 cells/well in 96-well plates with a U bottom, which had previously been coated with a 1% agarose gel film (used to prevent cell adherence to the bottom). After being plated, the cells were maintained in appropriate culture medium for each cell type, at 37 °C in a 5% CO2 humidified environment. The time for the formation of spheroids was 2 to 4 days of culture. After 12 culture days, spheroids were treated with zinc chloride and maintained in culture (with treatment) over a period of 24 h.

The treatment solutions were obtained using RPMI culture medium with 10% fetal bovine serum for tumorigenic cells and culture medium keratinocyte-SFM (KSF9) for normal RWPE-1 cells. Both culture media were supplemented with zinc chloride solution ($ZnCl_2$) at four concentrations: 0, 50, 100 and 150 μM. For the μXRF analysis, after 12 days of culture and periods of treatment, the spheroids were fixed in 4.0 % paraformaldehyde for 30 min, washed 3 times with 0.1 M phosphate buffered saline, pH 7.4, and then kept in phosphate buffered saline until the time of analysis. Before analysis, the spheroids were washed with Milli-Qwater and deposited on a 4 μm thick ultralene film, and then left to dry at room temperature.

2.2. Experimental setup

Analyses were performed in line D09B-XRF at the National Synchrotron Light Laboratory by μXRF technique with SR (μSRXRF). The samples were placed in a holder located 45 ° to the detector and to the incident beam that is, positioning 45 °/45 °. The image plane of the samples had an accuracy of 0.5 μm with three axes (X, Y, and Z) controlled by step motors.

The samples were excited using a white beam, 25 μm of extension vertically and 12 μm horizontally, achieved by a micro focus KB system. The step size was 25 μm/step in both directions and the acquisition time 300 ms/pixel. For the detection of the characteristic X-rays emitted from each pixel, we used a silicon drift detector with a resolution of 165 eV at 5.9 keV positioned at 90 ° with respect to the incident beam. The two-dimensional maps were obtained after normalization of the intensities of characteristic X-ray lines to the value of the ionization chamber. Figure 1 shows the experimental arrangement.

Figure 1: *Experimental arrangement for a synchrotron X-ray microfluorescence measurement.*

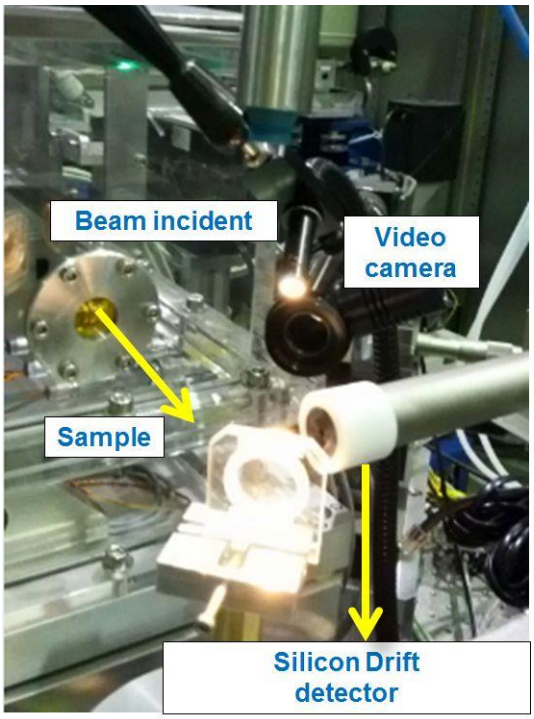

2.3. Data processing

The software GraphPad Prism 6 was used for data analysis and statistical tests. For analysis of the copper and iron distributions, three samples of each treatment and of each cell type were used in all the graphics and the data were normalized for the median value of the control (0 μM). The statistical differences between treatments were verified by the Kruskal-Wallis nonparametric test with a 5% level of significance.

X-ray microfluorescence spectra analysis was performed using PyMCA (Python Multichannel Analyzer) which is a free distributed software for non-commercial applications developed to process X-ray fluorescence data, in particular to decompose fluorescence signals into contributions of lines of the constituent parts of the sample [13].

3. RESULTS AND DISCUSSION

Figure 2 below shows an XRF spectrum of a prostatic cell spheroid. The technique allowed to detect the following elements: P, S, Cl, Ar, Ca, Fe, Cu and Zn, from the mentioned experimental conditions.

Figure 2: *X-ray fluorescence spectrum of normal cell spheroid.*

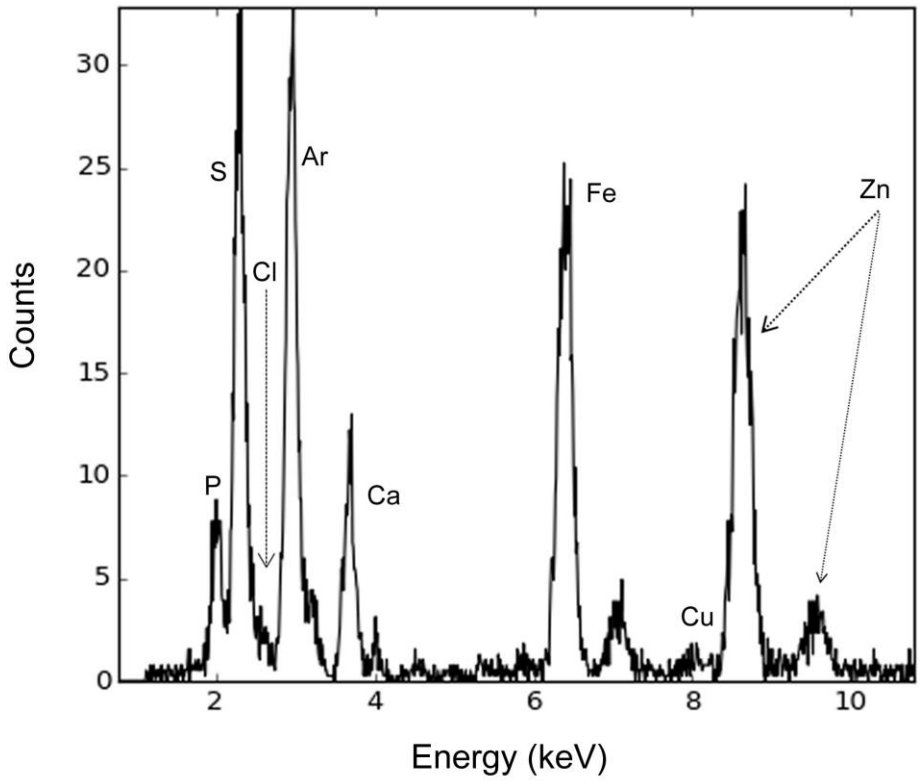

The presence of the Ar element in the spectrum was noted, since the experiment was carried out in a normal atmosphere, this is air, containing approximately 1.0 % Ar. Despite the elements detected, only Copper and Iron are of interest in this study.

The images of Figures 3 e 4 represent the two-dimensional intensity maps of copper and iron respectively, in the spheroids of tumorigenic cell lines supplemented with concentrations of 0 μM, 50

μM, 100 μM and 150 μM zinc chloride for 24 hours. The color scale depicts the intensity of the element in the spheroids, the red color represents the area in which this intensity is greater, the Cu and Fe intensities of each spheroid was normalized by its maximum value and the axes are in micrometers.

Figure 3: *Images resulting from two-dimensional intensity maps of Cu in tumorigenic spheroids with 0, 50, 100 and 150 μM of $ZnCl_2$ for 24 hours*

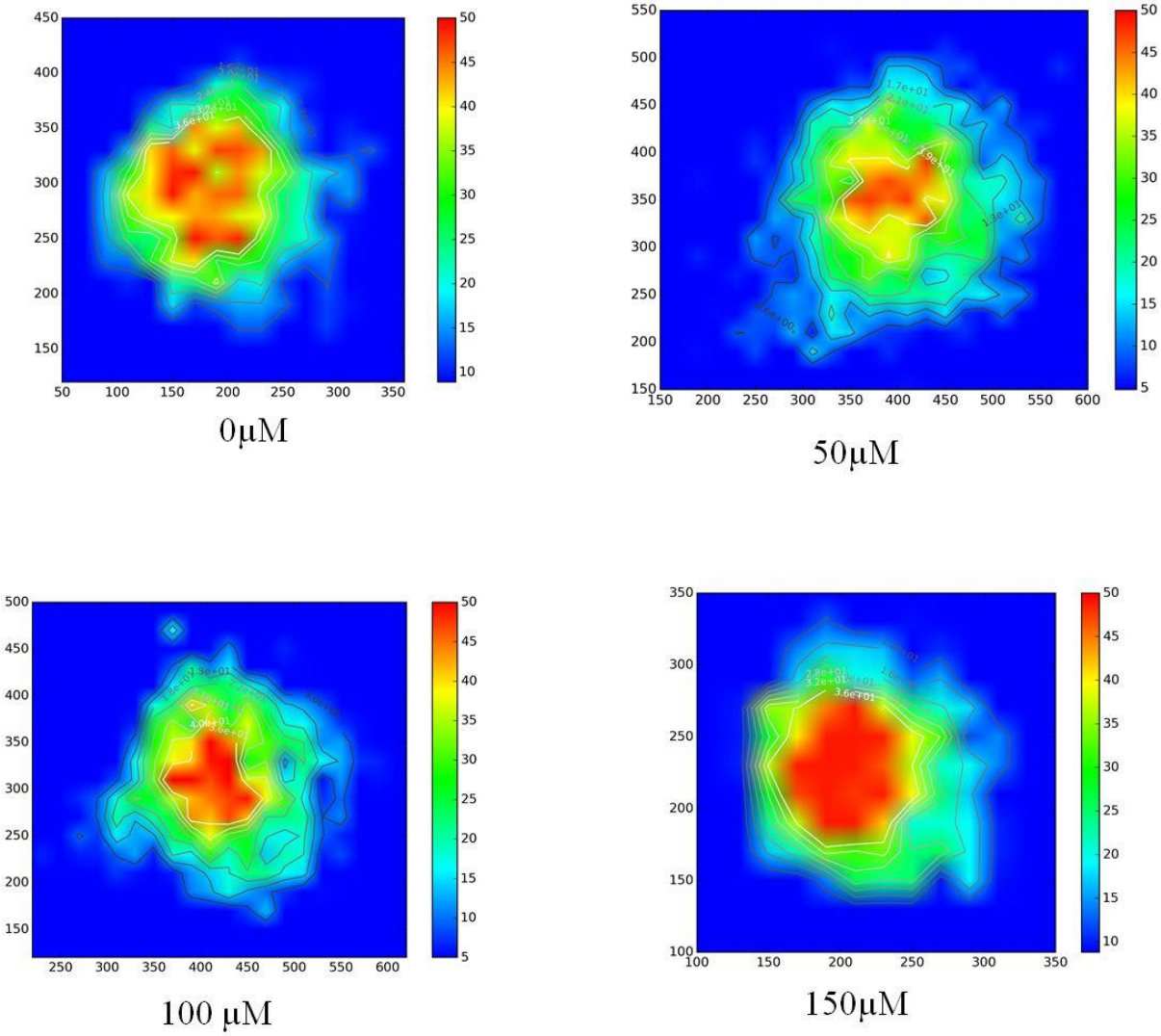

Figure 4: *Images resulting from two-dimensional intensity maps of Fe in tumorigenic spheroids with 0, 50, 100 and 150 µM of $ZnCl_2$ for 24 hours*

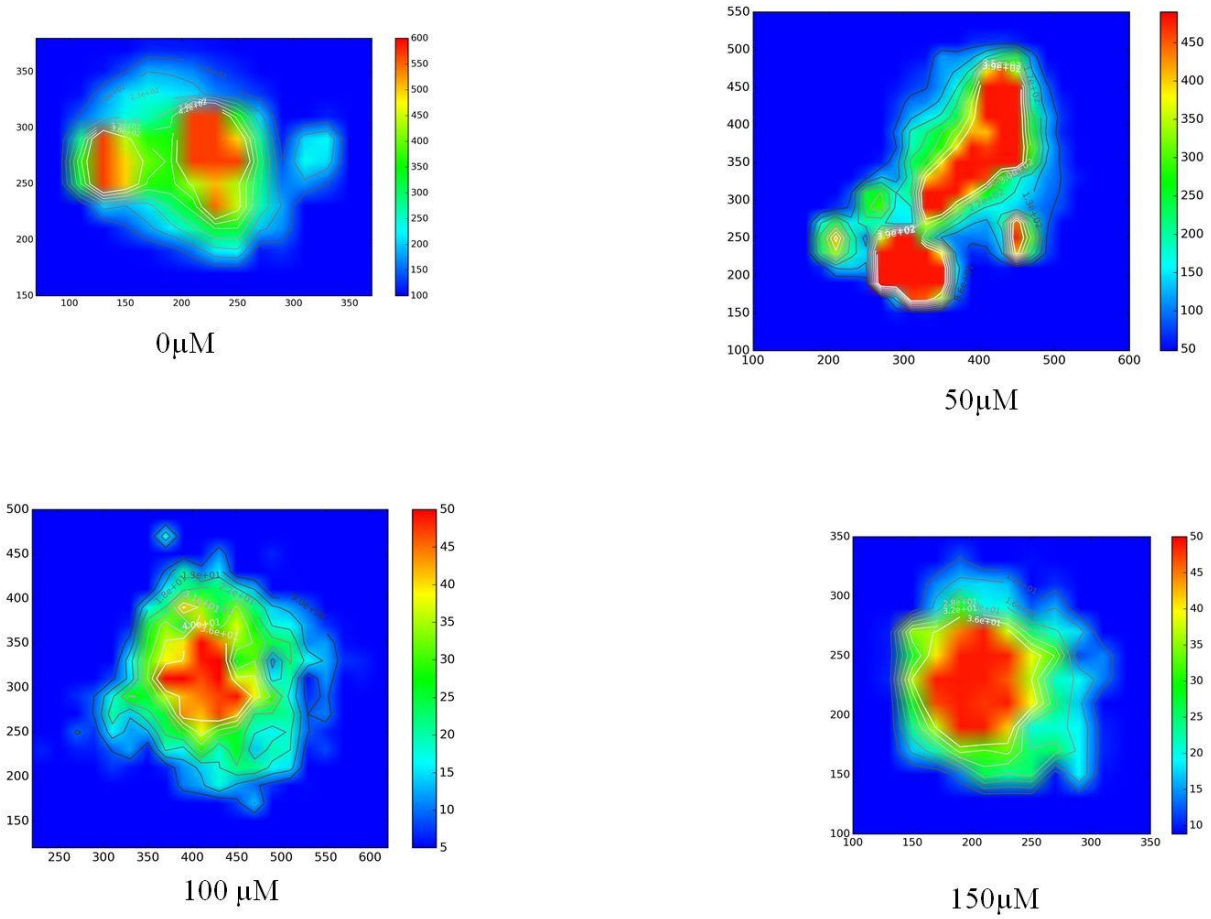

Figure 3 shows that the copper intensity in the spheroids of the tumorigenic cells is higher in the center and in the treatment of 150 µM the more intense area is larger. The intensity of iron has the same behavior, according to the images of figure 4. It may be noted that the geometry of the spheroids of tumor cell line is close to spherical.

The images in Figure 5 and 6 are the two-dimensional intensity maps of copper and iron, respectively, in normal cell line spheroids supplemented with concentrations of 0 µM, 50 µM, 100 µM and 150 µM zinc chloride for 24 hours.

Figure 5: *Images resulting from two-dimensional intensity maps of Cu in normal spheroids with 0, 50, 100 and 150 µM of $ZnCl_2$ for 24 hours*

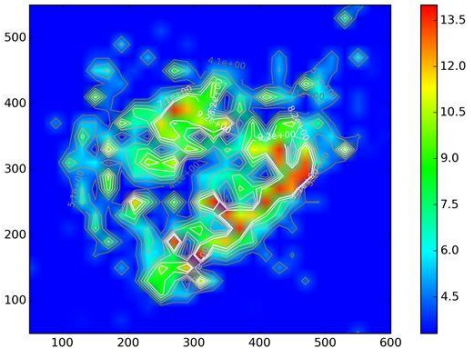

0µM

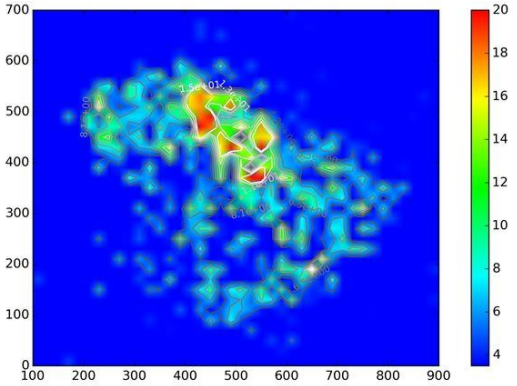

50µM

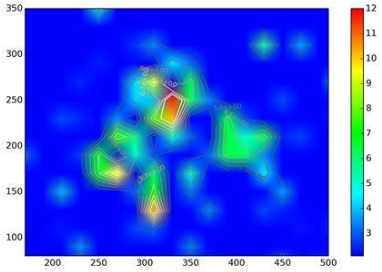

100 µM

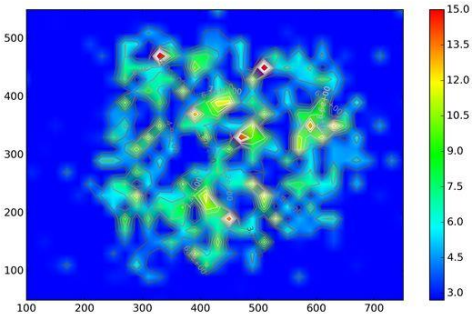

150µM

Figure 6: *Images resulting from two-dimensional intensity maps of Fe in normal spheroids with 0, 50, 100 and 150 µM of $ZnCl_2$ for 24 hours*

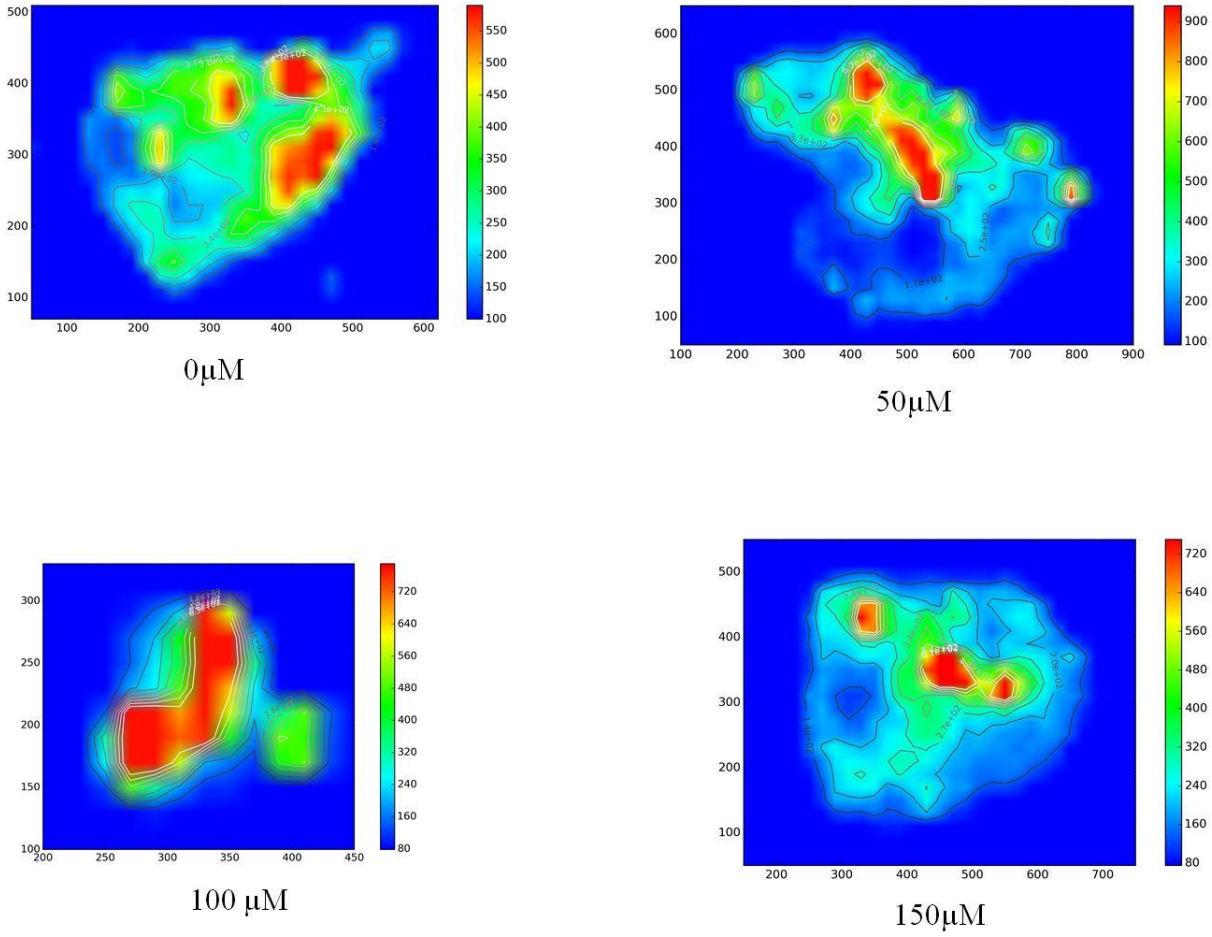

Figure 5 shows that the copper intensity in normal cells is not constant by the extension of the spheroid and that there are small points of high intensity. The iron intensity is higher in certain regions of the spheroid, but these more intense regions did not follow a position pattern, according to figure 6. The geometry of the spheroids of normal cell line is irregular.

Figure 7 show the variation of copper intensity according to the treatment of zinc chloride in tumor and normal cells, respectively, and Figure 8 show the variation of iron intensity. The results marked with an asterisk are above the level of significance (5 % level of significance), that is, $p > 0.05$, when compared with the control median.

Figure 7: *Normalized Copper intensity in (a) tumorigenic cell spheroids and (b) normal cell spheroids treated with $ZnCl_2$ for 24 hours*

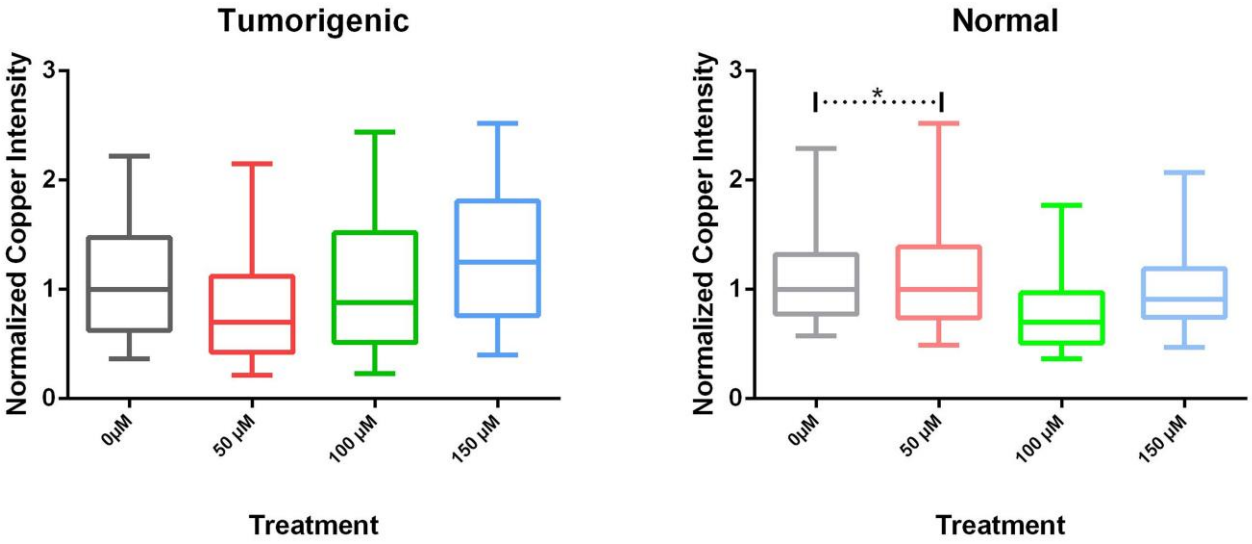

Figure 8: *Normalized Iron intensity in (a) tumorigenic cell spheroids and (b) normal cell spheroids treated with $ZnCl_2$ for 24 hours*

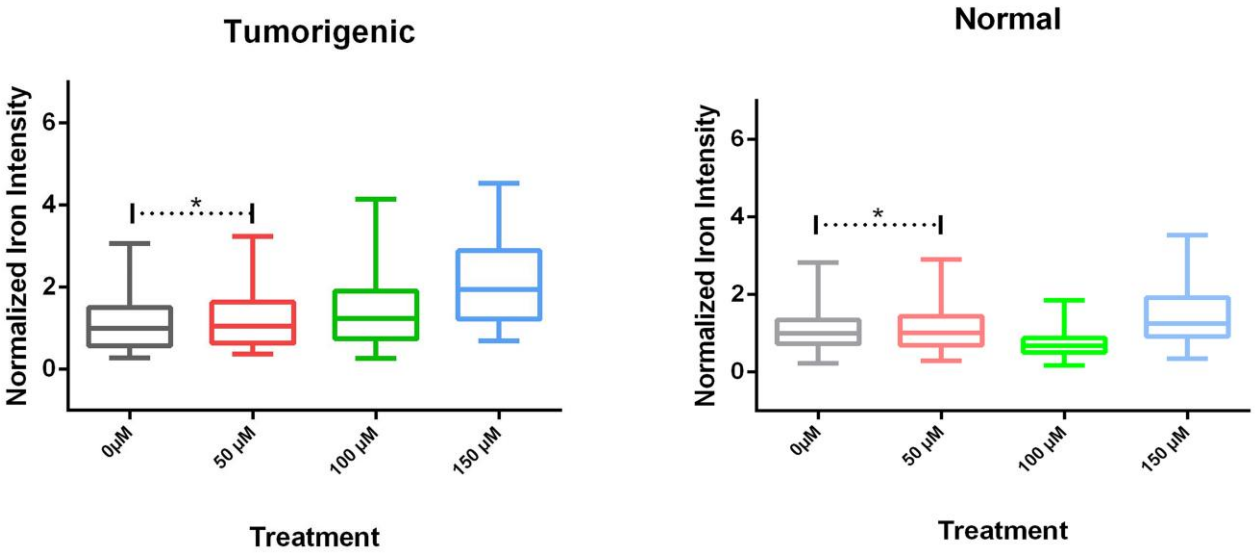

According to figure 7 (a), there was a decline in the intensity of copper in the tumor cells in the treatment of 50 µM, in the treatment of 100 µM there is an increase compared to the treatment of 50 µM, however the median of the copper intensity is still lower when compared to the control, and in 150 µM there were an increase when compared to the control. It was observed that the highest intensities were observed in the treatments of 150 µM. In the normal cells, figure 7 (b), the intensity of copper did not present a standard with respect to the treatment of zinc chloride, however the intensity remained lower in all the treatment when compared to the control.

Figure 8 (a) shows that the median iron intensity increased from the treatment of 100 µM in the tumor cell, whereas in normal cells the spheroids did not present a behavior pattern in relation to the treatment of zinc chloride, according to with Figure 8 (b). Table 1 shows the results using the Kruskal-Wallis test.

Table 1: Normalized intensity: Kruskal-Wallis test.

$ZnCl_2$ treatment	**Tumor**		**Normal**	
	Cu	**Fe**	**Cu**	**Fe**
	P-value	**P-value**	**P-value**	**P-value**
0 µM x 50 µM	< 0.0001	0.3425	> 0.9999	0.2990
0 µM x 100 µM	0.0283	< 0.0001	< 0.0001	< 0.0001
0 µM x 150 µM	0.0003	< 0.0001	< 0.0001	< 0.0001
50 µM x 100 µM	0.0283	< 0.0001	< 0.0001	< 0.0001
50 µM x 150 µM	0.0003	< 0.0001	< 0.0001	< 0.0001
100 µM x 150 µM	< 0.0001	< 0.0001	< 0.0001	< 0.0001

5 % level of significance

The results of MTT assay [14] showed no significant difference between the spheroids in the control group and those receiving treatment, suggesting that the viability of the cell didn't change regardless of treatment in both cell types analyzed, which allowed to conclude that apoptosis was not occurring.

The role of copper in the aetiology and growth of tumours has been extensively studied over the last two decades based initially on reports that serum and tumour levels of the metal are significant-

ly elevated in cancer patients compared to healthy subjects. Copper-ionophores that elevate intracellular bioavailable copper display significant therapeutic utility against prostate cancer cells in vitro [2,4]. In this study, it was observed that there was a reduction in copper intensity in treatments of 50 µM and 100 µM compared to the control.

Iron in cancer patients in view of the fact that in patients with chronic diseases or cancer, iron regulation and homeostasis are often distorted. This may result in insufficient iron supply to erythroblasts with clinical sequelae of iron deficiency such as weakness, fatigue, and impaired physical fitness and wellbeing as well as anemia [6]. Ferroportin protein is an important regulator of body iron metabolism, and is a membrane transport protein that transfers intracellular iron to the extracellular environment. Reduced expression levels of ferroportin on the cell surface lead to an increase in intracellular free iron, making the tumor cells more aggressive [15]. The iron intensity in the tumor cell increased from the treatment of 100 µM of zinc chloride.

Then zinc chloride may be a tool to increase the intracellular concentration of iron in cancer patients and decrease the intracellular concentration of copper. Further studies are needed to correlate this behavior with treatment with zinc chloride.

4. CONCLUSION

The microfluorescence technique was efficient in analyzing cell culture samples in three dimensions (spheroids). In this study, it can be noted that there was a decline in the intensity of copper in the tumor cells in the treatment of 50 µM and in the treatments of 100 and 150 µM there was an increase when compared to the control and it was observed that the highest intensity were in the treatment of 150 µM, that is, initially the treatment with zinc chloride aided in the reduction of the copper intensity, but the later treatments helped in the increase of the intensity of this metal. In the normal cells, the intensity of copper did not present a standard with respect to the treatment of zinc chloride, however the intensity remained lower in all the treatment when compared to the control. The iron intensity in the tumor cell increased from the treatment of 100 µM of zinc chloride.

This way, a different behavior was exhibit in relation the copper and iron capitation by normal and tumor prostatic cell lines, suggesting that ours model may represent an important tool to understanding the mechanisms of disease development and progression.

ACKNOWLEDGMENT

This study was supported in part by the National Council for Scientific and Technological Development (CNPq), the Rio de Janeiro State Research Foundation (FAPERJ) and the National Synchrotron Light Laboratory (LNLS) (Project XRF – 18905).

REFERENCES

[1] INCA - National Cancer Institute José Alencar Gomes da Silva. **Estimate 2016: Cancer Incidence in Brazil**. 2016. Available at: <http:// http://www.inca.gov.br/wcm/dncc/2015/estimativa-2016.pdf>. Last accessed: 27 July. 2017.

[2] GOUGH, M.; BLANTHORN-HAZELL, S.; DELURY, C.; PARKIN, E. The E1 copper binding domain of full-length amyloid precursor protein mitigates copper-induced growth inhibition in brain metastatic prostate cancer DU145 cells. **Biochemical and Biophysical Research Communications**, v. 453, p. 741-747, 2014.

[3] DENOYER, D.; CLATWORTHY, S.A.S.; MASALDAN, S.; MEGGYESY, P.M.; CATER, M.A. Heterogeneous copper concentrations in cancerous human prostate tissues. **The Prostate**, v. 75, p. 1510-1517, 2015.

[4] DENOYER, D.; PEARSON, H.B.; CLATWORTHY, S.A.S.; SMITH, Z.M.; FRANCIS, P.S.; LLANOS, R.M.; VOLITAKIS, I.; PHILLIPS, W.A.; MEGGYESY, P.M.; MASALDAN, S.; CATER, M.A. Copper as a target for prostate cancer therapeutics: copper-ionophore pharmacology and altering systemic copper distribution. **Oncotarget**, v. 7, p. 37064-37080, 2016.

[5] SAFI, R.; NELSON, E.R.; CHITNENI, S.K.; FRANZ, K.J.; GEORGE, D.J.; ZALUTSKY, M.R.; MCDONNELL, D.P. Copper Signaling Axis as a Target for Prostate Cancer Therapeutics. **Cancer Research**, v. 74, p.5819-5831, 2014.

[6] LUDWIG, H.; EVSTATIEV, R.; KORNEK, G.; AAPRO, M.; BAUERNHOFER, T.; BUXHOFER-AUSCH, V.; FRIDRIK, M.; GEISSLER, D.; GEISSLER, K.; GISSLINGER, H.; KOLLER, E.; KOPETZKY, G.; LANG, A.; RUMPOLD, H.; STEURER, M.; KAMALI, H.; LINK, H. Iron metabolism and iron supplementation in cancer patients. **Wiener Klinische Wochenschrift**, v. 127, p. 907-919, 2015.

[7] RODRIGO, M.; ZÍTKA, O.; ADAM, V.; KIZEK, R. Zinc and metallothionen in prostate cancer: A review. **Journal Of Metallomics And Nanotechnologies**, v. 2, p. 58-63, 2015.

[8] COSTELLO, L.C.; FRANKLIN, R.B. A comprehensive review of the role of zinc in normal prostate function and metabolism; and its implications in prostate cancer. **Archives Of Biochemistry And Biophysics**, v. 611, p. 100-112, 2016.

[9] JOHNSON, L.A.; KANAK, M.A.; KAJDACSY-BALLA, A.; PESTANER, J.P.; BAGASRA, O. Differential zinc accumulation and expression of human zinc transporter 1 (hZIP1) in prostate glands. **Methods**, v. 52, p. 316-321, 2010.

[10] LANKOSZ, M.; SZCZERBOWSKA-BORUCHOWSKA, M.; CHWIEJ, J.; OSTACHOWICZ, J.; SIMIONOVICI, A.; BOHIC, S. Research in quantitative microscopic X-ray fluorescence analysis. **Spectrochimica Acta Part B: Atomic Spectroscopy**, v. 59, p. 1517-1521, 2004.

[11] RAK, M.; SALOME, M.; KAMINSKYJ, S.G.W.; GOUGH, K.M. X-ray microfluorescence (μXRF) imaging of Aspergillus nidulans cell wall mutants reveals biochemical changes due to gene deletions. **Analytical And Bioanalytical Chemistry**, v. 406, p. 2809-2816, 2014.

[12] SANTINI, M.T.; RAINALDI, G. Three-Dimensional Spheroid Model in Tumor Biology. **Pathobiology**, v. 57, p. 148-157, 1999.

[13] SOLÉ, V.; PAPILLON, E.; COTTE, M.; WALTER, PH.; SUSINI, J. A multiplatform code for the analysis of energy-dispersive X-ray fluorescence spectra. **Spectrochimica Acta Part B: Atomic Spectroscopy**, v. 62, p.63-68, 2007.

[14] ROCHA, K.M.J.; LEITÃO, R.G.; OLIBEIRA-BARROS, E.G.; OLIVEIRA, M.A.; CANELLAS, C.G.L.; ANJOS, M.J.; NASCIUTTI, L.E.; LOPES, R.T. Zinc distribution in

human prostate carcinoma cell line using synchrotron X-ray microfluorescence. **X-Ray Spectrometry**, v. 46, p. 403-411, 2017.

[15] XUE, D.; ZHOU, C.X.; SHI, Y.B.; LU, H.; HE, X.Z. Decreased expression of ferroportin in prostate cancer. **Oncology Letters**, v. 10, p. 913-916, 2015.